UNIVERSITÀ DI PARMA
ARCHIVIO DELLA RICERCA

University of Parma Research Repository

Selectively Absorbing Small-Molecule Solar Cells for Self-Powered Electrochromic Windows

note finali coverpage

(Article begins on next page)

03 February 2025

Selectively Absorbing Small-Molecule Solar Cells for Self-Powered Electrochromic Windows

Xiangkun Jia[1,#], Elizabeth Christine Baird[1,#], Jan Blochwitz-Nimoth[1], Sebastian Reineke[1,*], Koen Vandewal[2,*], Donato Spoltore[1,*]

[1] *Dresden Integrated Center for Applied Physics and Photonic Materials (IAPP) and Institute for Applied Physics, Technische Universität Dresden, Nöthnitzer Str. 61, 01187 Dresden, Germany*
[2] *Institute for Materials Research (IMO-IMOMEC), Hasselt University, Wetenschapspark 1, 3590 Diepenbeek, Belgium*

[#] These authors contributed equally: Xiangkun Jia, Elizabeth Christine Baird
[*] Corresponding authors

E-mail addresses: (sebastian.reineke@tu-dresden.de, koen.vandewal@uhasselt.be, donato.spoltore@tu-dresden.de)

Abstract

Dynamic control of solar transmission by photovoltaic-powered electrochromic smart windows is an up-and-coming approach towards the reduction of energy consumption in buildings. Selectively-absorbing transparent organic solar cells are capable of exhibiting excellent visible-light transparency as well as respectable power conversion efficiencies. This work presents three different transparent small-molecule solar cells (TSCs) with an area of 2.52 cm^2, two of which are UV-absorbing and one of which absorbs in the NIR, each in combination with an organic electrochromic device (EC). The NIR-absorbing TSC uses a BDP-OMe:C$_{60}$ combination, and has a power conversion efficiency of 4% with an average visible light transmission (AVT) of 40%. The two UV-harvesting systems, α-6T/B4PYMPM and NPB:B4PYMPM, each have an AVT of 50-65%, as well as high open-circuit voltages of 1.5-2.0 V. We demonstrate that these photogenerated voltages are sufficient to power a fluoran dye-based organic EC, which has excellent optical properties: its color ranges from highly transparent to deep black, and its on/off contrast ratio is higher than 80% in the range between 390 nm and 640 nm. Self-powered smart windows made by the combination of TSCs and ECs provide a way to significantly reduce energy consumption from air conditioning and lighting, towards zero-energy buildings.

1. Introduction

Heating, air conditioning, and lighting in buildings account for a major portion of electricity demand, around 40% of overall energy usage as of 2018 [1]. With the effects of climate change rapidly worsening, it is imperative that we find ways to reduce this energy burden. Adaptation of PV technology into building-integrated photovoltaics (BIPV), which act as self-powering temperature-regulating building envelopes, could help to alleviate this issue in different ways [2,3]. BIPV can minimize long-distance transmission losses and installation costs by generating electricity close to where it is utilized, for example on roofs, facades, and solar shading systems [4]. One especially promising branch of BIPV involves electrochromic smart windows powered by transparent photovoltaic modules. These self-sufficient devices regulate the transmission of solar radiation through building windows, controlling the interior climate without increasing energy usage [5–7]. By reducing the amount of electricity required to manage indoor temperature and lighting, these devices can help to mitigate the overall energy consumption, thereby contributing to fight climate change. In this paper, we will present a BIPV system consisting of a combination of an electrochromic device (EC) and transparent solar cells (TSCs), each of which can be easily fabricated from organic materials.

In order to create a self-sustaining TSC-EC module, the power conversion efficiency (PCE) and average visible light transmission (AVT) of TSCs need to be balanced [8]. Transparent polymer solar cells with PCEs of 3-13% have been demonstrated in the past with AVTs in the range of ~ 10-50% [8–14]. However, when using blade coating method to increase those devices' active area over 1 cm^2, their fill factors, photocurrents and PCEs drop, indicating scalability problems and limited usefulness in larger applications [15–18]. The selectively absorbing small-molecule

61   TSCs presented here have superior AVTs and scalability potential compared to polymer-based

62   transparent solar cells [19]. Among them, the near-infrared (NIR)-absorbing TSCs with an area

63   of 2.52 cm^2 exhibit, to the best of our knowledge, the highest PCE ($\sim$ 4%) in combination with

64   an AVT of 40%, compared to other reported small-molecule based TSCs [20–23]. While the

65   near-ultra-violet (UV) absorbing TSCs offer photovoltages of 1.5-2.0 V, enough to control light

66   transmission through the EC devices, the NIR devices require a series connection to achieve

67   sufficiently high voltages. However, the larger photocurrent ($\sim$ 10 mA cm^{-2}) achieved by the

68   NIR TSCs in comparison with that of near-UV TSCs partially compensates for their lack of

69   photovoltage. The UV-absorbing TSCs have outstanding AVTs of up to 65%, along with

70   excellent solar heat gain coefficient (SHGC) values reaching 60%. The SHGC values indicate

71   that these UV-absorbing TSCs are good candidates for powering EC windows in colder

72   climates where additional heating is advantageous. On the other hand, the NIR-harvesting

73   device would provide more benefit in hot climates, since they block some of the IR radiation to

74   prevent the indoor from overheating.

75   Most commercially available electrochromic technologies operate by an electrochemical

76   oxidation/reduction reaction between inorganic metal oxide thin films, usually tungsten and

77   nickel oxide [24–27]. The EC system presented here diverges from this traditional configuration.

78   Instead of metal oxides, it is based on a type of dye commonly referred to as fluoran. Fluoran

79   dyes have been widely utilized as a component of thermal paper, and are reported as the active

80   agent in a handful of reports on EC devices [28,29]. Fluoran-based EC systems have been

81   studied most extensively by the Information Display group at Kyung-Hee University. They

82   have investigated the use of fluoran EC in several applications, including as a component in

83 augmented reality headsets and as part of an OLED-EC combination [30,31]. However, fluoran

84 EC has yet to be reported in smart window applications. Studies on the optical properties of this

85 material for ECs have shown that the performance of fluoran derivatives are comparable to

86 those of commercially available electrochromic windows, which offer a transparent-state

87 transmittance of 65%-78% and a darkened-state transmittance of 1%-4% [32].

88 **2. Experimental section**

89 *2.1. Sample preparation*

90 *2.1.1. Small-molecule solar cells preparation*

91 The layers of the small-molecule solar cells are thermally evaporated at ultra-high vacuum (base

92 pressure $< 10^{-7}$ mbar) on a glass substrate with a pre-structured ITO contact (Thin Film Devices,

93 USA). Glass substrates are cleaned in a multi-step wet process including rinsing with N-methyl-

94 2-pyrrolidone, ethanol, and deionized water as well as treatment with ultraviolet ozone. The

95 performances of the small molecule solar cells are optimized for opaque devices, before making

96 them transparent. The optimization steps are shown in Figure S1-3 and Table S1-3. In order to

97 make the optimized devices transparent, the thickness of the top Ag electrode is reduced from

98 100 to 7 nm. The structures of devices and of the used materials for all transparent solar cells

99 are listed in Table S4. All organic materials are purified 2-3 times by sublimation. The device

100 area is defined by the geometrical overlap of the bottom and the top contact, the active area of

101 standard and large-area devices equals 6.44 mm^2 and 2.52 cm^2, respectively. To avoid exposure

102 to ambient conditions, the organic part of the device is covered by a small glass substrate, which

103 is glued on top.

2.1.2. Organic electrochromic devices preparation

The electrochromic solution contains chemical components in the following approximate

concentrations: 0.3M tetrabutylammonium tetrafluoroborate, 0.5M black fluoran dye and 0.5M

hydroquinone in N,N-dimethylacetamide. All chemicals are used as received from the

manufacturer. Devices are all made with two pieces of ITO glass and the EC thickness is

determined by tape spacer.

2.2. Characterization techniques

Current-voltage characteristics in dark and under solar illumination are measured with an SMU

(Keithley 2400, USA) at room temperature in ambient conditions. The cells are illuminated

with a spectrally mismatch corrected intensity of 100 mW cm^{-2} (AM1.5g) provided by a sun

simulator (16 S-150 V.3 Solar Light Co., USA). The intensity is monitored with a Hamamatsu

S1337 silicon photodiode (calibrated by Fraunhofer ISE Freiburg, Germany).

EQE$_{PV}$ measurements are taken using masks to minimize edge effects and to define an exact

photoactive area (2.78 mm²). The *EQE*$_{PV}$ is detected with a lock-in amplifier (Signal Recovery

SR 7265) under monochromatic illumination (Oriel Xe Arc-Lamp Apex Illuminator combined

with Cornerstone 260 1/4m monochromator, Newport, USA) using a calibrated mono-

crystalline silicon reference diode (Hamamatsu S1337 calibrated by Fraunhofer ISE, Germany).

Transmission and reflection spectra for transparent solar cells and electrochromic devices are

measured by Shimadzu UV-3100 and Shimadzu solid-spec 3700 spectrometers. In order to

measure the transmission spectra for transparent standard devices with an area of 6.44 mm², a

mask is used to make sure that light pass through from the transparent active layer region only.

125 For large-area TSCs (2.52 cm^2), we measure transmission and reflection spectra in the range

126 between 300 to 2500 nm for the calculation of SHGC. In order to measure the transmission

127 spectra of EC devices at different applied voltages, the devices are mounted inside the UV-Vis

128 spectrometer while being wire-connected to an external power source, a Keithley 2602 SMU

129 or a transparent solar cells. With these spectra, CRI and CIE coordinates are calculated by

130 ColorCalculator software produced by OSRAM Sylvania, Inc. SHGC values are obtained by

131 utilizing the equations mentioned in Note S1.

132 **3. Results and discussion**

133 *3.1. Chemical structures and optoelectronic properties of small-molecule TSCs*

134 The transparent solar cells use combinations of electron-donating and electron-absorbing

135 materials whose chemical structures, energy levels, and absorption spectra are shown in Fig. 1.

136 The materials NPB and α-6T are utilized as electron donors. The ionization potential (IP) and

137 electron affinity (EA) levels of the high-gap material NPB are 5.46 and 2.45 eV respectively

138 [33], resulting in an absorption peak at around 347 nm as shown in Fig. 1c. The IP and EA of

139 α-6T are 5.0 and 3.0 eV respectively [34], with an optical gap around 2.0 eV and a relatively

140 broad absorption region from 330 to 550 nm (see Fig. 1c). The absorption of NPB is localized

141 in the UV region, while α-6T also absorbs visible light. B4PYMPM works as an electron

142 acceptor when combined with NPB or α-6T, lending to a subtle contribution to the light

143 absorption while providing interfaces with both donor materials which efficiently dissociate

144 excitons into free carriers [35]. For devices absorbing in the NIR, BDP-OMe is combined with

145 C$_{60}$. As a narrow-gap (~ 1.44 eV) small-molecule material shown in Fig. 1b, BDP-OMe has a

strong absorption peak at around 800 nm, making it a satisfactory NIR photon absorber. The absorption of BDP-OMe in the visible regions is quite weak, which is beneficial to the transmission of visible light.
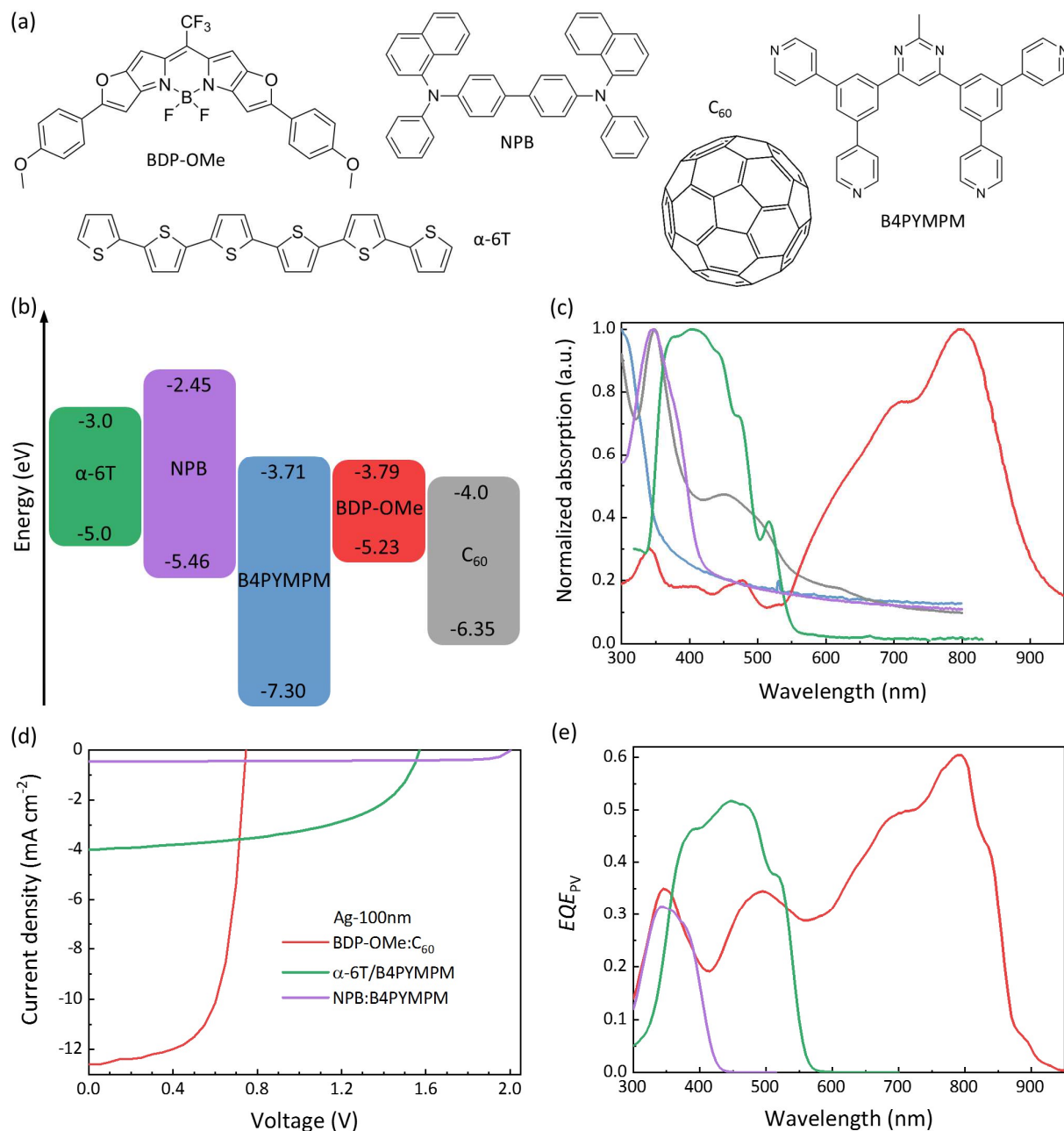
Fig. 1. (a) Chemical structures, (b) Energy levels, and (c) Normalized UV-Vis absorption spectra of the materials used in this work. The energy levels of α-6T [34], NPB [33], B4PYMPM [36], and C_{60} [37] are obtained from the literature. (d) Current-density voltage (J-V) characteristics, and (e) Photovoltaic external quantum efficiency (EQE_{PV}) for solar cells with 100 nm thick Ag electrodes. The area of the active layer of the studied solar cells is 6.44 mm^2.
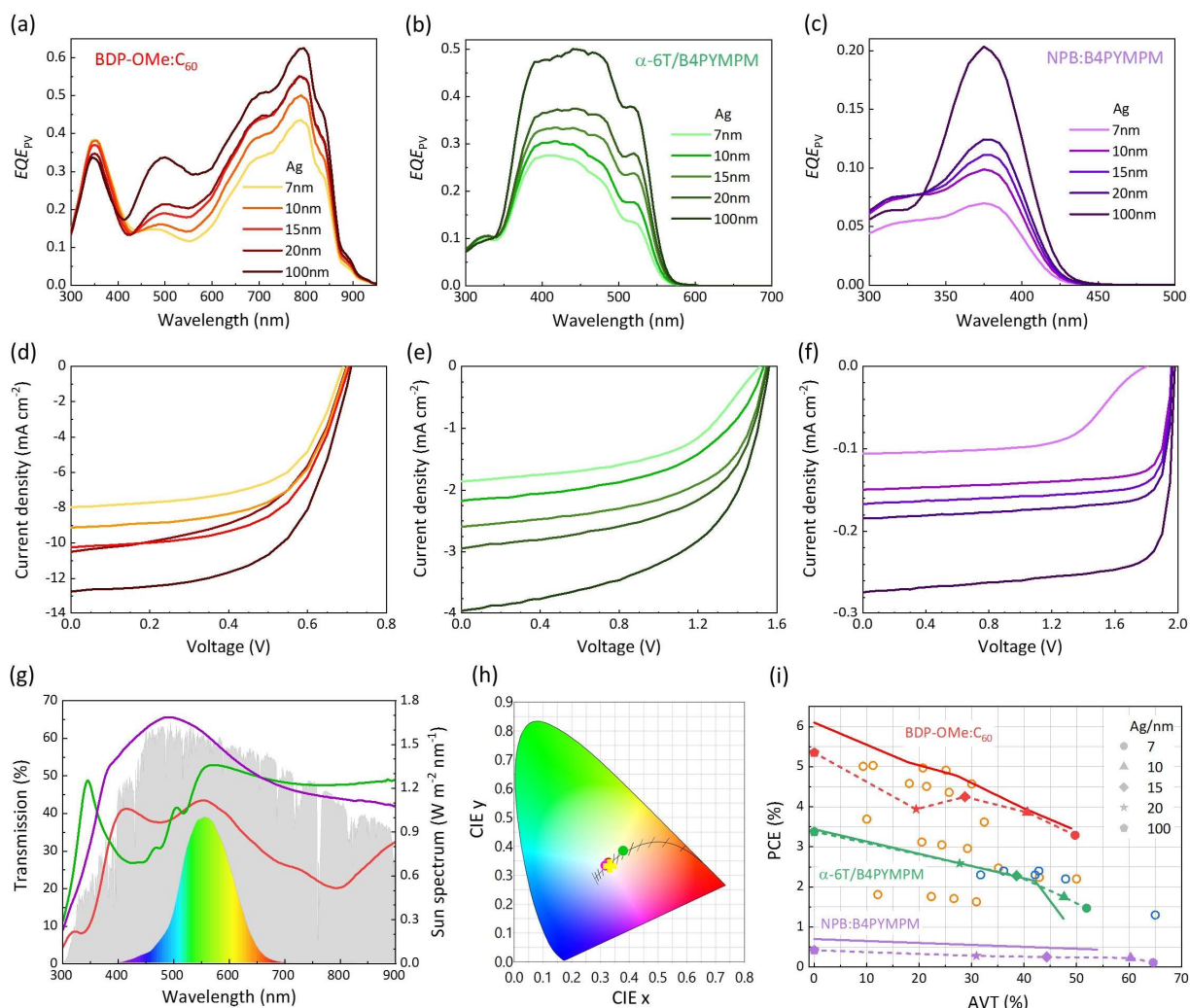
3.2 Photovoltaic performance of TSCs

Current-voltage characteristics of bulk and planar heterojunction (BHJ/PHJ) solar cells are measured under simulated solar intensity (AM 1.5g). Fig. 1d-e show the photovoltaic performance of 6.44 mm^2 opaque solar cells with 100 nm-thick Ag electrodes. The photovoltaic parameters, along with the performance of devices with various thicknesses of Ag electrodes, are summarized in Figure S4 and Table S5. For the near-UV light-harvesting devices, open-circuit voltages (V_{OC}) as high as 1.57 V and 2.00 V are achieved in the planar α-6T/B4PYMPM and bulk NPB:B4PYMPM junction, with fill factors (*FF*) of 54.6% and 76.3%, respectively. For the α-6T devices, a higher performance is obtained for planar junction than for bulk heterojunction devices (Figure S2 and Table S2). Due to its higher external quantum efficiency (*EQE*$_{PV}$), the performance of the α-6T device is superior to that of the NPB device, with a short-circuit current density (J_{SC}) of 4.0 mA cm^{-2} and a corresponding PCE of 3.44%. When the thickness of the Ag electrode is reduced to 10 nm, to make the device transparent, the PCE of α-6T/B4PYMPM and NPB:B4PYMPM decreases to 1.21% and 0.44%, respectively. This is mainly due to the diminished J_{SC} from reduced absorption in the active layers, resulting from the curtailed back reflection from the Ag top electrode. Interestingly, the V_{OC} of the device with the reduced-thickness Ag electrode remains unaffected. For the BHJ NIR-absorbing solar cell, BDP-OMe:C$_{60}$ has a dramatically enhanced J_{SC} of 12.58 mA cm^{-2}, which is consistent with both its broad and high *EQE*$_{PV}$ and the fact that the sunlight provides more photons in the spectral region where this device has the strongest absorption. The PCE of this BDP-OMe containing device reaches 6.10%, with a *FF* of 64.9% and a V_{OC} of 0.75 V. When the thickness of the Ag electrode is reduced to 10 nm, the maximum *EQE*$_{PV}$ drops to 48%, with a corresponding drop

177   in J_{SC} and PCE to 8.98 mA cm^{-2} and 3.97%. However, the values for V_{OC} and FF remain nearly

178   unchanged. The stability of those devices is also very important. Recent reports confirmed that

179   organic solar cells have operation times of several years [38], in particular thermally evaporated

180   devices exhibit enhanced stability compared to their solution-processed competitor [39].

181   *3.3 Scalability of NIR/UV-absorbing TSCs*

182   In order to demonstrate the scalability of the vacuum deposition technique used for these TSCs,

183   devices with active areas above one square centimeter are fabricated. Fig. 2 shows the

184   photovoltaic characteristics as well as the transmission and reflection spectra of these enlarged

185   devices. The performance of BDP-OMe:C$_{60}$ device drops by around 10% when the active area

186   is raised from 6.44 mm^2 to 2.52 cm^2. This is mainly due to the slightly-lowered V_{OC} and FF,

187   the latter of which may result from the increased resistance of the larger ITO electrode [40].

188   However, this effect is nearly absent in the α-6T/B4PYMPM devices. The PCE of large-area α-

189   6T-based opaque devices reaches 3.38 %, with a V_{OC} of 1.56 V, J_{SC} of 3.95 mA cm^{-2}, and FF of

190   54.9%, similar to the photovoltaic parameters of the small-area device. The V_{OC} and FF of the

191   NPB:B4PYMPM system remain unchanged when scaling up the device area to 2.52 cm^2, but

192   the J_{SC} decreases from 0.46 to 0.27 mA cm^{-2}, resulting in a PCE that is diminished to 0.42%.

193   When the thicknesses of Ag electrodes are minimized to achieve transparent devices, the

194   photovoltaic performance of TSCs is reduced mainly because of a loss of back reflection and

195   an increased sheet resistance of the Ag film [41]. Nevertheless, the efficiencies of both the BDP-

196   OMe- and α-6T-based devices remain adequate even with 10 nm-thick Ag electrodes: 3.86%

197   for BDP-OMe and 1.75% for α-6T. To the best of our knowledge, the FF of the

198 NPB:B4PYMPM system presented here, which reaches up to 77.7% in a device with an active

199 area of 2.52 cm^2 and a 10 nm thick Ag film, is the highest value among reported transparent

200 small-molecule solar cells [20,21,42,43].

201

Fig. 2. Photovoltaic and optical performance of large-area (2.52 cm^2) small-molecular solar
cells with varied thickness of Ag. (a, b, c) Photovoltaic external quantum efficiency (*EQE*$_{PV}$)
and (d, e, f) Current density - voltage (*J-V*) characteristics. Pictures of those large-area samples
are shown in Figure S5. (g) Transmission spectra for large-area transparent solar cells with 10
nm thick Ag electrodes. The photopic response of the human eye is also shown in rainbow
colors. (h) The international commission on illumination CIE 1931 (x, y) coordinates of the
transmission spectra for all transparent solar cells with 10 nm thick Ag electrode. Red symbols
represent the BDP-OMe:C$_{60}$ combination, green symbols represent α-6T/B4PYMPM devices,
and purple symbols represent the NPB:B4PYMPM cells. The yellow cross represents the white
light (0.333, 0.333). (i) PCE vs AVT plot for all investigated small-molecule solar cells. Solid
lines indicate the performance of devices with a standard active-area of 6.44 mm^2, symbol-dash
lines represent large-area devices. The reported transparent small-molecule solar cells

214 processed via solution and thermal evaporation are shown in orange and blue open circles,
215 respectively [20–23].

216 *3.4 Optical and thermal properties of TSCs*

217 In addition to the photovoltaic performance, the amount of visible light and solar energy

218 transmitted through the TSC is ascertained by determining their AVT, color rendering index

219 (CRI), and solar heat gain coefficient (SHGC). The reflection and transmission spectra of

220 devices with transparent Ag electrodes are shown in Figure S6, and corresponding values for

221 the AVT, CRI, and SHGC are shown in Table 1. The AVT through the device is calculated

222 based on the transmission $T(\lambda)$ by the following formula [44]:

223
$$\text{AVT} = \frac{\int_{390}^{830} T(\lambda)P(\lambda)S(\lambda)\mathrm{d}(\lambda)}{\int_{390}^{830} P(\lambda)S(\lambda)\mathrm{d}(\lambda)}, \tag{1}$$

224 where λ is the wavelength and $S(\lambda)$ is the solar spectrum (AM1.5g). The photopic spectral

225 luminous efficiency function $P(\lambda)$ describes the average spectral sensitivity of human vision in

226 regard to brightness [45].

227 The trends shown in Table 1 make it apparent that reducing the electrode thickness greatly

228 enhances the AVT. With a 10 nm thick Ag electrode, the AVT values for the two UV-absorbing

229 TSCs are excellent: 60.3% for NPB:B4PYMPM, and 47.6% for α-6T/B4PYPMPM. The NIR-

230 absorbing combination BDP-OMe:C_{60} has a decent AVT value of 40%, and has the highest PCE

231 (~ 4%) of the three devices. These BDP-OMe:C_{60} devices show the best efficiency-to-AVT

232 trade-off, with performances that are comparable or superior to previously-reported results in

233 the field of transparent small-molecule solar cells in Fig. 2i [20–23]. Moreover, it has been

234 demonstrated that, when shifting the absorption peaks of molecules from visible to NIR region,

13

235 the reduction of PCE in order to get an equivalent AVT (~ 30%) is diminished from 25% to

236 15% [20]. The main absorption peaks of our devices are not located in the visible region. As a

237 result, this selectively UV/NIR-absorbing property makes the performance reduction of our

238 devices smaller than devices that utilize non-selective absorbers as shown in Figure S7. These

239 results indicate that selectively harvesting sunlight is one way to ameliorate the loss of

240 performance in transparent solar cells.

241 **Table 1.** Photovoltaic and optical performance of large-area (2.52 cm^2) photovoltaic devices.

|	Ag (nm)	V_{OC} (V)	J_{SC} (mA cm^{-2})	*FF* (%)	*PCE* (%)	AVT (%)	CRI	CIE 1931 (x, y)	SHGC
BDP-OMe: C$_{60}$	7	0.69	7.96	60.0	3.29	49.7	94	0.3398, 0.3505	0.46
	10	0.70	9.12	60.4	3.86	40.6	94	0.3274, 0.3430	0.37
	15	0.71	10.24	59.0	4.25	28.7	93	0.3112, 0.3303	0.28
	20	0.70	10.49	53.7	3.94	19.4	93	0.2974, 0.3171	0.22
	100	0.71	12.74	59.1	5.35				
α-6T/ B4PYMPM	7	1.51	1.86	52.0	1.47	51.9	95	0.3766, 0.3812	0.56
	10	1.53	2.17	52.6	1.75	47.6	93	0.3793, 0.3852	0.48
	15	1.55	2.59	56.8	2.28	38.6	90	0.3624, 0.3788	0.31
	20	1.55	2.94	56.7	2.59	27.7	89	0.3515, 0.3729	0.24
	100	1.56	3.95	54.9	3.38				
NPB: B4PYMPM	7	1.80	0.11	59.4	0.11	64.6	98	0.3329, 0.3404	0.60
	10	1.96	0.15	77.7	0.23	60.3	99	0.3179, 0.3338	0.47
	15	1.96	0.17	77.7	0.25	44.3	98	0.2980, 0.3188	0.33
	20	1.96	0.18	77.9	0.28	30.9	98	0.2821, 0.3024	0.24
	100	1.98	0.27	77.3	0.42				

242 The CRI is a parameter used to quantitatively describe how accurately a light source or

243 transparent medium reproduces the color of a given object, in comparison with the same object

244 illuminated by an ideal light source (e.g. AM 1.5g) [46]. A CRI of 100 would indicate perfect

245 color reproduction. All three of the transparent devices presented here have excellent CRI

246 values, over 93 in the case of devices with 10 nm thick electrodes, indicating remarkable color-

247 rendering qualities. The CIE 1931 (x, y) coordinates of transmission spectra for the transparent

248   BDP-OMe:C_{60} and NPB:B4PYMPM devices approach those of the solar spectrum as the Ag

249   electrode becomes thinner (Figure S6).

250   In addition to their optical properties, the amount of solar heat energy our TSCs are able to

251   transmit is also significant for BIPV applications. The SHGC, whose value ranges from 0 to 1,

252   is a parameter that can be used to assess the thermal transfer properties of TSCs [47]. The higher

253   a window's SHGC, the more solar energy it can transmit [48]. The SHGC values for all of our

254   TSCs are strongly correlated with the thickness of the Ag electrode, devices with thinner

255   electrodes have higher SHGC values. The NIR-absorbing BDP-OMe:C_{60} cells are the best at

256   blocking incoming heat, as evidenced by their relatively low SHGC figures compared to the

257   UV-absorbing cells. Its SHGC values are less affected by the reduction in electrode thickness

258   than those for UV-absorbing α-6T/B4PYMPM and NPB:B4PYMPM, which stems from the

259   ability of BDP-OMe:C_{60} to convert more long-wavelength light into electricity than the UV

260   absorbing-devices, thereby reducing the amount of solar energy allowed into the indoor

261   environment. This heat-blocking ability makes BDP-OMe:C_{60}-based devices best suited for use

262   in hot climates, as they can help reducing electricity consumption due to air conditioning [49].

263   The near UV-absorbing solar cells have a lower heat-blocking ability, indicated by their higher

264   SHGCs. These values go up to 60%, which is comparable to a typical double-glazed window

265   (> 60%) [50]. This would make devices based on α-6T/B4PYMPM and NPB:B4PYMPM more

266   appropriate for cooler areas, since they help preserving heat by allowing more NIR light to pass

267   through, thereby keeping the room warm [49].

268   *3.5 Electrochromic devices*

269 Organic EC materials have been used in a variety of applications, including self-dimming

270 mirrors and goggles [51], displays [52], and electrochromic e-skins [53]. The organic EC

271 technology described here has distinctive properties, offering a superior on-off contrast ratio

272 along with a low-cost, solution-based fabrication process [30]. Instead of metal oxide layers,

273 the color-switching medium consists of a dye-containing liquid that changes from invisible to

274 black by either electrochemical oxidation or an acid/base reaction [54]. The device itself runs

275 on a low DC voltage that can be provided by the transparent solar cells described in the previous

276 section. The combination of TSCs with ECs offers a promising option for sustainable light and

277 temperature control in residential or office buildings [55].
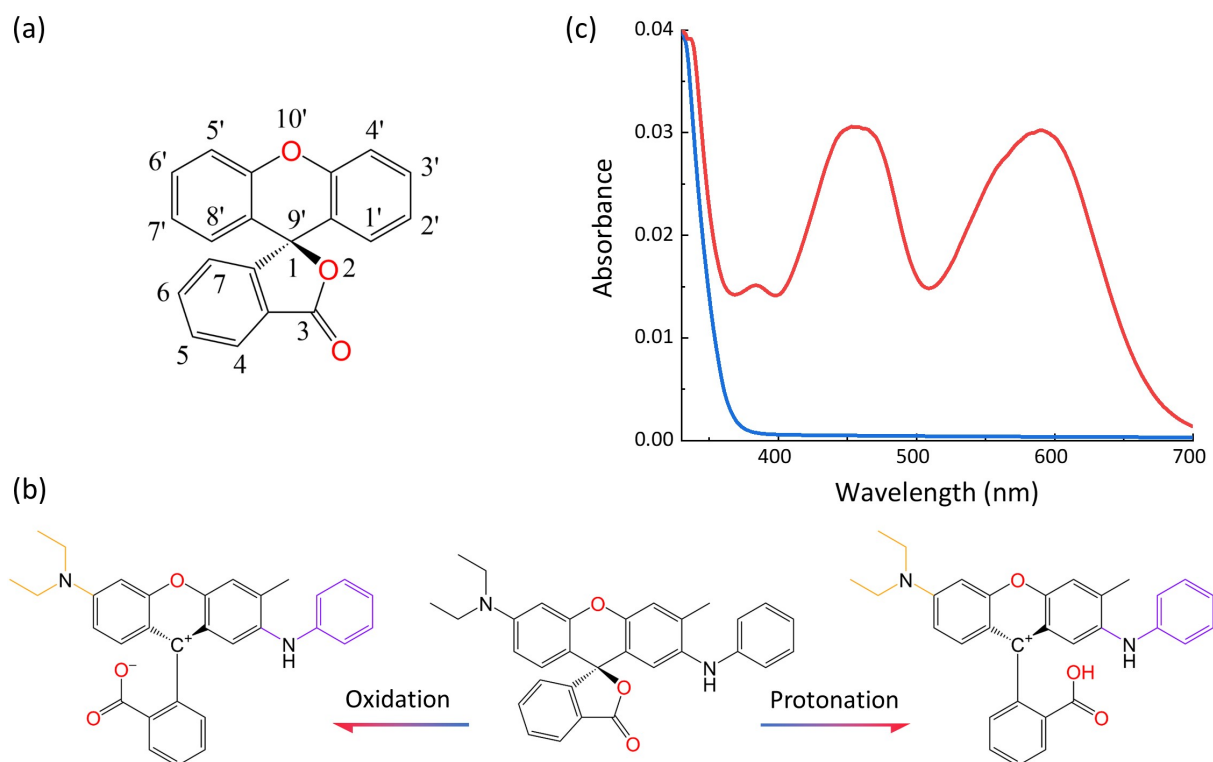
278

279 **Fig. 3.** Properties and coloration mechanism of fluoran dye. (a) The core structure of a fluoran
280 dye molecule. (b) The transparent, closed-ring molecule can be switched to black by either
281 oxidation (left) or protonation (right). (c) Absorption spectra of black fluoran dye in its
282 transparent (blue curve) and its darkened states (red curve). The black color stems from the
283 absorption in the whole visible light range, in particular two absorption peaks, one in the violet
284 and one in the yellow region, each of which is associated with separate functional groups

285 attached to the fluoran dye core. In the case of black fluoran dye, the groups are attached to the
286 6' and 2' positions [56].

287 The electrochromic pigment utilized here belongs to the family of fluoran dyes. Fluoran dyes
288 all share the same core molecular structure as shown in Fig. 3a, and the final color is determined
289 by the type and position of functional groups attached to the core [56]. Switching these dyes
290 from transparent to colored is done by cleaving the lactone ring, specifically the bond between
291 9' and 2 positions. Breaking this bond changes the hybridization of the spiro-carbon from sp^3
292 to sp^2, extending the conjugated π-electron system and shifting the HOMO-LUMO level into
293 the visible range [49,57]. This bond-breaking coloration mechanism comes about in our devices
294 via a combination of two different pathways, depicted in Fig. 3b. One is by electrochemical
295 oxidation, wherein coloration occurs upon exposure of the dissolved dye to an electric field
296 [30]. In our devices, this happens by diffusion of the dye molecules to the working electrode.
297 The other coloration pathway is via direct protonation in a Bronsted-Lowry acid/base reaction,
298 where a free H^+ ion binds with the oxygen atom in the lactone ring, thereby breaking the C-O
299 bond and extending the molecule's π-conjugation [58,59]. The free H^+ ions in our devices come
300 from the oxidation of hydroquinone at the working electrode, which creates benzoquinone and
301 H^+ ions. The bleaching of this device occurs by the inverse of the coloration process.
302 Electrochemical reduction and/or deprotonation of the dye molecule closes the lactone ring and
303 resets the dye to its transparent state. Interestingly, this bleaching can happen at either a negative
304 or a neutral bias. The bleaching at 0 V is much slower than at negative bias, because at neutral
305 bias the molecules have to diffuse all the way to the counter-electrode for reduction and
306 deprotonation. At a negative bias, these processes occur directly at the working electrode, so
307 there is no additional wait for diffusion time [30].

308   A black-hued fluoran dye was chosen for our devices, in part for its excellent optical qualities,

309   and also because it is easily obtained and for example already used ubiquitously in thermal

310   paper (e.g., printed receipts) [56]. The dye's black color stems from the combination of

311   absorption throughout the visible wavelengths in addition to two maxima, found in the yellow

312   and in the violet wavelengths (see Fig. 3c). One maximum occurring around 450 nm is

313   associated with the anilino functional group at the 2' position, and imparts a violet color. The

314   other maximum around 600 nm comes from the alkyl functional group at the 6' position, giving

315   a yellow color. The absorption over the whole visible region, presenting in particular two

316   maxima in the yellow and violet region, results in a black hue.[56,60]
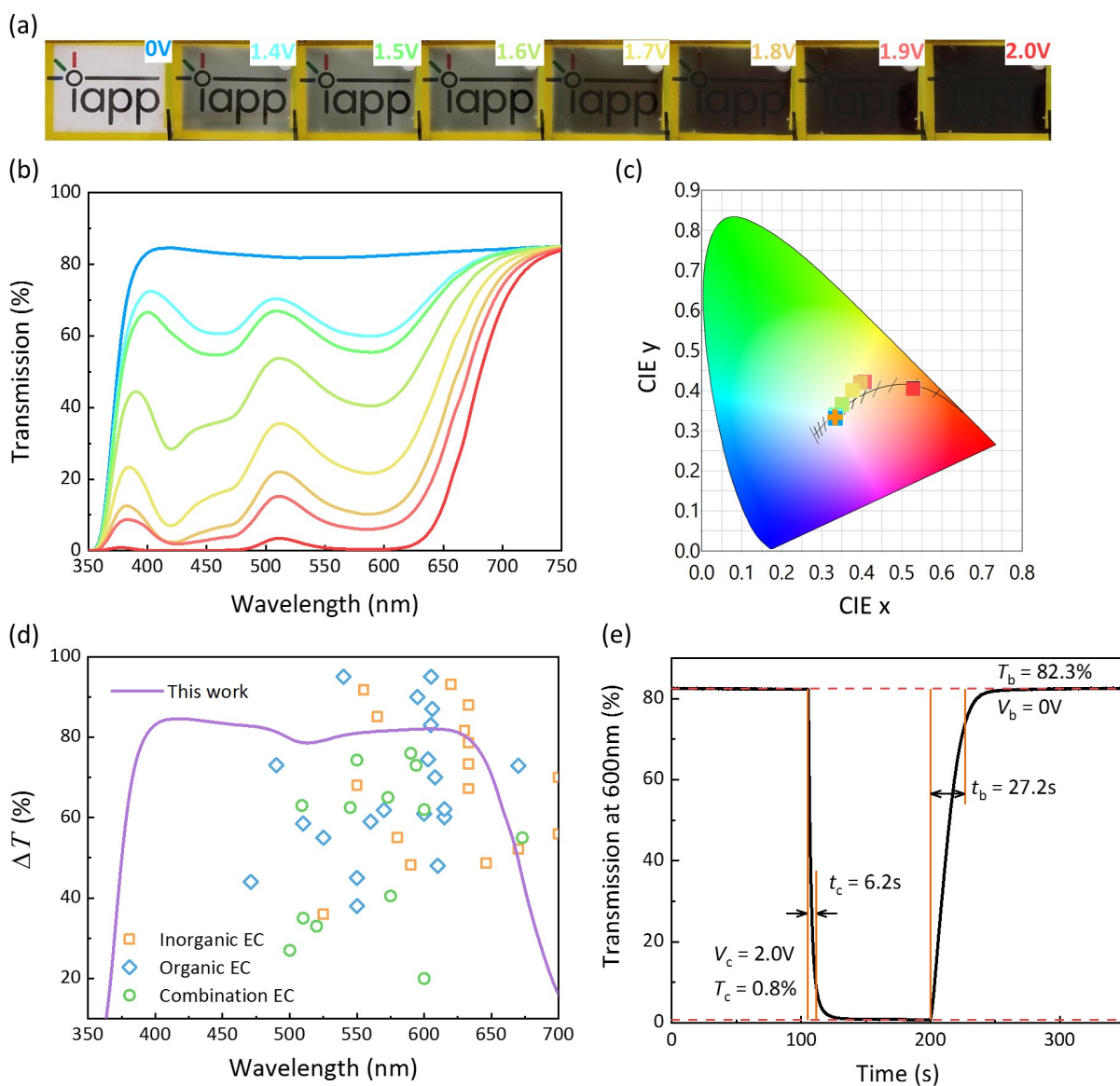
Fig. 4. Electrochromic device performances. (a) Photographs and (b) Transmission spectra of a 70 μm-thick EC device held at the same voltage levels as in (a). A Keithley 2602 SMU is used to apply voltages to the EC device and to manipulate its transmission properties. (c) The CIE 1931 (x, y) coordinates of the device in each state when holding voltage changes from 0V to 2V stepwise. Different colors indicate varied turn-on voltages. The coordinate of the solar spectrum as a reference is shown as an orange cross. (d) Comparison of transmission difference (ΔT) between bleached state and darkened state in various types of EC devices. Details can be found in Table S6. (e) Bleaching and coloration times of the EC device extracted for a 90% of transmission change, from which the calculation of the coloration efficiency is shown in Note S2.

Fabrication of an EC device from dihydroxybenzene and fluoran dye involves simply

dissolving the components in a solvent along with an electrolyte salt, then sealing the resulting

liquid between two sheets of ITO glass. Fig. 4a shows a 70 μm-thick EC device operated by

331 applying a DC voltage (1.4-2.0 V) to switch the color from clear to deep black, the transmission

332 spectra of which are shown in Fig. 4b. The transmission in the unbiased off-state is very high

333 throughout the visible wavelengths, with an AVT of 82.2%. The fully opaque on-state transmits

334 very little light, with an AVT of 1.7%. Moreover, as shown in Fig. 4d, a high contrast ratio of

335 over 80% can be obtained in the range of 390 to 640 nm, which is comparable or higher than

336 those of commercially available EC smart windows [32]. This EC device can also offer varying

337 shades of black that still allow a portion of visible light to filter through, depending on the initial

338 amount of applied voltage. For a less-intense shade of black, one only needs to use a switching

339 voltage lower than 2 V. A noticeable variance between shades can be seen with about a 0.1 V

340 difference in switching potential. Lighter shades are achieved by applying switching potentials

341 of 1.4-1.6 V, and darker shades come from switching at 1.7-1.9 V. The color quality for each

342 of the states is represented in the CIE (x, y) coordinate plot in Fig. 4c. The EC device in the

343 fully-transparent state has coordinates of (0.333, 0.331), very close to those of the solar

344 spectrum. This indicates that the device in the off-state has a very clear and neutral color quality

345 which is further evidenced by the CRI value of 94 shown in Table S7.

346 In addition to the contrast ratio between bleached and colored states, switching speed and

347 coloration efficiency are two important metrics to evaluate the performance of EC devices [27].

348 The switching on and off times for 90% transmission change are extracted, as shown in Fig. 4e.

349 Upon applying a driving voltage of 2.0 V, the EC device needs a coloration time (t_c) of 6.2 s to

350 reach a darkened state. However, since no reversed voltage is applied to revert the EC device

351 back to a transparent state, the bleaching time (t_b) is longer, 27.2 s. It is worth noticing that a

352 negative bias can indeed speed up the bleaching process: the t_b is decreased to 11.2 s when an

353 -1 V bias is applied (see Figure S8). The coloration efficiency represents the change in

354 transmission contrast divided by charges consumed per unit of active EC area [7,61]. Compared

355 to inorganic EC devices which have coloration efficiencies in the range of 19 to 133 cm^2 C^{-1}

356 [5,7,27], the coloration efficiency of our organic EC device is excellent and can reach up to

357 147.6 cm^2 C^{-1} when its 90% optical density change is achieved. About the stability of our EC

358 devices, several works report that similar fluoran dye based devices exhibit transmittances of

359 bleached and colored states losses below 10% even after 12,000 cycles [30,62,63].

3.6 Self-powered electrochromic smart window

361 We demonstrate now the capability of TSCs to power EC devices in order to manipulate their

362 transmission state. Photographs of EC and EC driven by TSCs are shown in Fig. 5a, and

363 corresponding transmission spectra and calculated optical parameters are shown in Fig. 5b and

364 Table S8. Because its output voltage at the maximum power point is ~ 0.55 V, NIR-absorbing

365 TSCs need to be series-connected to get sufficient voltage to drive the EC device. As shown in

366 Fig. 5a, two series-connected NIR TSCs can only partly dim the EC, while three NIR devices

367 are able to make the transmission change very distinct with AVT and CRI reduced from 82.2%

368 to 19.7% and 93 to 73, respectively. Conversely, NPB-containing TSCs need a parallel

369 connection to produce enough current to make the coloration reaction in the EC device happen.

370 The power density of a single large-area α-6T TSCs under 1 sun intensity is sufficient to drive

371 the EC device because the energy consumption of the EC device is as low as 2.7 W m^{-2} when

372 it is held at 1.6 V as shown in Figure S9. The low energy dissipation of the organic EC makes

373 the self-powered TSC+EC stack possible. The aforementioned stack is made by combining a

374 2.52 cm² α-6T containing TSC with a 70 μm-thick EC device with an area of 2.85 cm². After

375 illumination, the transmission of the organic EC is lowered as shown in Fig. 5d. It is worth to

376 note that the EC can be tuned to a deep darkened state when two series-connected 6T TSCs are

377 employed (see Fig. 5a), which indicates that with the help of well-designed circuit and other

378 electric elements such as resistors, the photovoltaic-powered, transmission-tunable

379 electrochromic window is indeed possible. This self-powered TSC+EC stack has great potential

380 to replace the most common double-glazed windows due to its feasibility in large-scale

381 manufacturing, easy installation, and energy-saving and sunlight-manipulating properties.
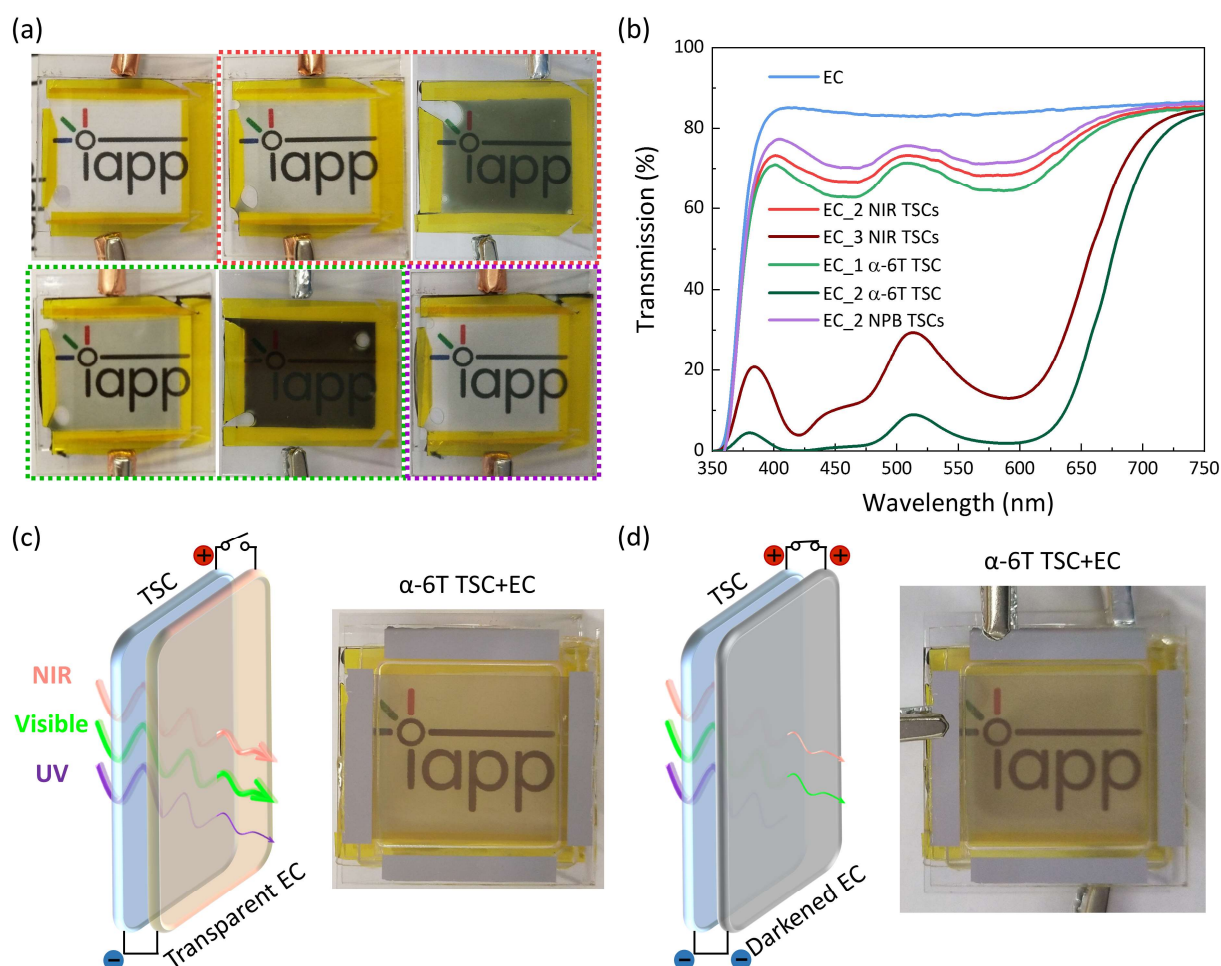
382

383 **Fig. 5.** Performance of electrochromic device driven by transparent solar cells. (a) The top left
384 shows an EC device at transparent state, the top right shows the EC powered by two or three
385 series-connected BDP-OMe:C₆₀ NIR TSCs respectively (red box) as demonstrated in Figure
386 S10. The EC charged by one or two α-6T/B4PYMPM TSCs are shown on the bottom left in a

green box and on the bottom right by two parallel-connected NPB:B4PYMPM TSCs, shown in a purple box. The illumination intensity for all the TSCs is ~1 sun. (b) Corresponding transmission spectra of the EC device manipulated by TSCs. (c) Schematic illustration of electrochromic smart window connected with transparent solar cells as a promising alternative to traditional double-glazed windows. The front view of the real stack of α-6T/B4PYMPM and EC is shown on the right. (d) Schematic illustration and real self-powered TSC+EC stack at the darkened state.

4. Conclusion

We have demonstrated a promising combination of transparent large-area (2.52 cm^2) small-molecule solar cells with a low-cost, solution-processed organic electrochromic device. Our UV-TSCs exhibit ample AVT and excellent color quality as well as high photovoltage (>1.5 V). The NIR-harvesting blend BDP-OMe:C$_{60}$ shows a PCE of ~ 4% with an AVT of ~ 40%, which are superior compared with reported small molecule based TSCs. UV/NIR TSCs in series or parallel connection are able to drive fluoran-based EC devices and to manipulate its AVT from 82.2% to 1.7%. Our results show that UV/NIR selectively absorbing TSCs are good candidates for power-generating windows without sacrificing the transmission of visible light. The EC device's remarkable on/off contrast ratio and adjustable transmission properties make these suitable for controlling the indoor climate, which is important to realize smart energy-efficient buildings. We hope this work will inspire more efforts into the synthesis of high-efficiency, selectively absorbing, PV materials, and more advanced techniques to enlarge the area of TSCs over 1 m^2 without significant performance reduction.

Author contributions

X.J., D.S., and K.V. designed the experiments, prepared photovoltaic devices, and optimized their performance. X.J. performed the J-V and EQE measurements for all solar cells. E.C.B. and X.J. prepared electrochromic devices and performed UV-Vis measurements for EC devices; X.J. did this measurement for transparent solar cells. J.B-N., S.R., K.V., and D.S. supervised their team members involved in this project. X.J. and E.C.B. wrote the manuscript. All authors contributed to the critical analysis of the findings and the revision of the manuscript. D.S supervised the overall project.

Competing interests

The authors declare no competing interests.

References

[1] A. Ghosh, B. Norton, Advances in switchable and highly insulating autonomous (self-powered) glazing systems for adaptive low energy buildings, Renew. Energy. 126 (2018) 1003–1031. https://doi.org/10.1016/j.renene.2018.04.038.

[2] A. Detollenaere - Becquerel Institute, Snapshot of Global PV Markets 2020 PVPS Task 1 Strategic PV Analysis and Outreach, 2020. www.iea-pvps.org (accessed September 2, 2020).

[3] B.P. Jelle, Building integrated photovoltaics: A concise description of the current state of the art and possible research pathways, Energies. 9 (2016) 1–30. https://doi.org/10.3390/en9010021.

[4] A. Cannavale, F. Martellotta, F. Fiorito, U. Ayr, The Challenge for Building Integration of Highly Transparent Photovoltaics and Photoelectrochromic Devices, Energies. 13 (2020) 1929. https://doi.org/10.3390/en13081929.

[5] C.J. Barile, D.J. Slotcavage, J. Hou, M.T. Strand, T.S. Hernandez, M.D. McGehee, Dynamic Windows with Neutral Color, High Contrast, and Excellent Durability Using Reversible Metal Electrodeposition, Joule. 1 (2017) 133–145. https://doi.org/10.1016/j.joule.2017.06.001.

[6] X.H. Li, C. Liu, S.P. Feng, N.X. Fang, Broadband Light Management with Thermochromic Hydrogel Microparticles for Smart Windows, Joule. 3 (2019) 290–302. https://doi.org/10.1016/j.joule.2018.10.019.

[7] H. Fang, P. Zheng, R. Ma, C. Xu, G. Yang, Q. Wang, H. Wang, Multifunctional hydrogel enables extremely simplified electrochromic devices for smart windows and ionic writing boards, Mater. Horizons. 5 (2018) 1000–1007. https://doi.org/10.1039/c8mh00856f.

[8] K. Lee, H. Um, D. Choi, J. Park, N. Kim, H. Kim, K. Seo, The Development of Transparent Photovoltaics, Cell Reports Phys. Sci. 1 (2020) 100143. https://doi.org/10.1016/j.xcrp.2020.100143.

[9] Y. Cui, C. Yang, H. Yao, J. Zhu, Y. Wang, G. Jia, F. Gao, J. Hou, Efficient Semitransparent Organic Solar Cells with Tunable Color enabled by an Ultralow-Bandgap Nonfullerene Acceptor, Adv. Mater. 29 (2017) 1–7. https://doi.org/10.1002/adma.201703080.

[10] W. Wang, C. Yan, T.-K. Lau, J. Wang, K. Liu, Y. Fan, X. Lu, X. Zhan, Fused Hexacyclic Nonfullerene Acceptor with Strong Near-Infrared Absorption for Semitransparent Organic Solar Cells with 9.77% Efficiency, Adv. Mater. 29 (2017) 1701308.

456   https://doi.org/10.1002/adma.201701308.

457   [11]   B. Jia, S. Dai, Z. Ke, C. Yan, W. Ma, X. Zhan, Breaking 10% Efficiency in Semitransparent Solar

458   Cells with Fused-Undecacyclic Electron Acceptor, Chem. Mater. 30 (2018) 239–245.

459   https://doi.org/10.1021/acs.chemmater.7b04251.

460   [12]   H. Chen, H. Lai, Z. Chen, Y. Zhu, H. Wang, L. Han, Y. Zhang, F. He, 17.1 %-Efficient Eco-

461   Compatible Organic Solar Cells from a Dissymmetric 3D Network Acceptor, Angew. Chemie.

462   132 (2020) 2–11. https://doi.org/10.1002/ange.202013053.

463   [13]   G.P. Kini, S.J. Jeon, D.K. Moon, Latest Progress on Photoabsorbent Materials for

464   Multifunctional Semitransparent Organic Solar Cells, Adv. Funct. Mater. 2007931 (2021)

465   2007931. https://doi.org/10.1002/adfm.202007931.

466   [14]   Z. Hu, J. Wang, X. Ma, J. Gao, C. Xu, K. Yang, Z. Wang, J. Zhang, F. Zhang, A critical review

467   on semitransparent organic solar cells, Nano Energy. 78 (2020) 105376.

468   https://doi.org/10.1016/j.nanoen.2020.105376.

469   [15]   X. Li, H. Meng, F. Shen, D. Su, S. Huo, J. Shan, J. Huang, C. Zhan, Semitransparent fullerene-

470   free polymer solar cell with 44% AVT and 7% efficiency based on a new chlorinated small

471   molecule acceptor, Dye. Pigment. 166 (2019) 196–202.

472   https://doi.org/10.1016/j.dyepig.2019.03.024.

473   [16]   W. Su, Q. Fan, X. Guo, J. Wu, M. Zhang, Y. Li, Efficient as-cast semi-transparent organic solar

474   cells with efficiency over 9% and a high average visible transmittance of 27.6%, Phys. Chem.

475   Chem. Phys. 21 (2019) 10660–10666. https://doi.org/10.1039/C9CP01101C.

476   [17]   E. Pascual-San-José, G. Sadoughi, L. Lucera, M. Stella, E. Martínez-Ferrero, G.E. Morse, M.

477   Campoy-Quiles, I. Burgués-Ceballos, Towards photovoltaic windows: scalable fabrication of

478   semitransparent modules based on non-fullerene acceptors via laser-patterning, J. Mater. Chem.

479   A. 8 (2020) 9882–9895. https://doi.org/10.1039/D0TA02994G.

480   [18]   J. Zhang, G. Xu, F. Tao, G. Zeng, M. Zhang, Y. (Michael) Yang, Y. Li, Y. Li, Highly Efficient

481   Semitransparent Organic Solar Cells with Color Rendering Index Approaching 100, Adv. Mater.

482   31 (2019) 1807159. https://doi.org/10.1002/adma.201807159.

483   [19]   M. Riede, D. Spoltore, K. Leo, Organic Solar Cells—The Path to Commercial Success, Adv.

484   Energy Mater. 2002653 (2020) 1–10. https://doi.org/10.1002/aenm.202002653.

485   [20]   D. Yang, T. Sano, H. Sasabe, L. Yang, S. Ohisa, Y. Chen, Y. Huang, J. Kido, Colorful Squaraines

486   Dyes for Efficient Solution-Processed All Small-Molecule Semitransparent Organic Solar Cells,

487   ACS Appl. Mater. Interfaces. 10 (2018) 26465–26472. https://doi.org/10.1021/acsami.8b08878.

488 [21] J. Min, C. Bronnbauer, Z.G. Zhang, C. Cui, Y.N. Luponosov, I. Ata, P. Schweizer, T. Przybilla,

489   F. Guo, T. Ameri, K. Forberich, E. Spiecker, P. Bäuerle, S.A. Ponomarenko, Y. Li, C.J. Brabec,

490   Fully Solution-Processed Small Molecule Semitransparent Solar Cells: Optimization of

491   Transparent Cathode Architecture and Four Absorbing Layers, Adv. Funct. Mater. 26 (2016)

492   4543–4550. https://doi.org/10.1002/adfm.201505411.

493 [22] R.R. Lunt, V. Bulovic, Transparent, near-infrared organic photovoltaic solar cells for window

494   and energy-scavenging applications, Appl. Phys. Lett. 98 (2011) 113305.

495   https://doi.org/10.1063/1.3567516.

496 [23] J. Meiss, F. Holzmueller, R. Gresser, K. Leo, M. Riede, Near-infrared absorbing semitransparent

497   organic solar cells, Appl. Phys. Lett. 99 (2011) 193307. https://doi.org/10.1063/1.3660708.

498 [24] N. DeForest, A. Shehabi, S. Selkowitz, D.J. Milliron, A comparative energy analysis of three

499   electrochromic glazing technologies in commercial and residential buildings, Appl. Energy. 192

500   (2017) 95–109. https://doi.org/10.1016/j.apenergy.2017.02.007.

501 [25] S.-I. Park, Y.-J. Quan, S.-H.S. Kim, H. Kim, S.-H.S. Kim, D.-M. Chun, C.S. Lee, M. Taya, W.-

502   S. Chu, S.-H. Ahn, A review on fabrication processes for electrochromic devices, Int. J. Precis.

503   Eng. Manuf. Technol. 3 (2016) 397–421. https://doi.org/10.1007/s40684-016-0049-8.

504 [26] X. Xia, Z. Ku, D. Zhou, Y. Zhong, Y. Zhang, Y. Wang, M.J. Huang, J. Tu, H.J. Fan, Perovskite

505   solar cell powered electrochromic batteries for smart windows, Mater. Horizons. 3 (2016) 588–

506   595. https://doi.org/10.1039/C6MH00159A.

507 [27] Y. Ke, J. Chen, G. Lin, S. Wang, Y. Zhou, J. Yin, P.S. Lee, Y. Long, Smart Windows: Electro-,

508   Thermo-, Mechano-, Photochromics, and Beyond, Adv. Energy Mater. 9 (2019) 1902066.

509   https://doi.org/10.1002/aenm.201902066.

510 [28] K. Kanazawa, K. Nakamura, N. Kobayashi, Electroswitchable optical device enabling both

511   luminescence and coloration control consisted of fluoran dye and 1,4-benzoquinone, Sol. Energy

512   Mater. Sol. Cells. 145 (2016) 42–53. https://doi.org/10.1016/j.solmat.2015.06.061.

513 [29] I.J. Ko, J.H. Park, G.W. Kim, R. Lampande, J.H. Kwon, An optically efficient full-color

514   reflective display with an electrochromic device and color production units, J. Inf. Disp. 20 (2019)

515   155–160. https://doi.org/10.1080/15980316.2019.1649310.

516 [30] G.W. Kim, Y.C. Kim, I.J. Ko, J.H. Park, H.W. Bae, R. Lampande, J.H. Kwon, High-Performance
517 Electrochromic Optical Shutter Based on Fluoran Dye for Visibility Enhancement of Augmented
518 Reality Display, Adv. Opt. Mater. 6 (2018) 1701382. https://doi.org/10.1002/adom.201701382.

519 [31] D.C. Choe, G.W. Kim, R. Lampande, J.H. Kwon, 54.4: Smart Window Devices for Black Screen
520 of Organic Light Emitting Diodes, SID Symp. Dig. Tech. Pap. 46 (2015) 821–823.
521 https://doi.org/10.1002/sdtp.10343.

522 [32] M. Casini, Active dynamic windows for buildings: A review, Renew. Energy. 119 (2018) 923–
523 934. https://doi.org/10.1016/j.renene.2017.12.049.

524 [33] J. Feng, F. Li, W. Gao, S. Liu, Y. Liu, Y. Wang, White light emission from exciplex using tris-(8-
525 hydroxyquinoline)aluminum as chromaticity-tuning layer, Appl. Phys. Lett. 78 (2001) 3947–
526 3949. https://doi.org/10.1063/1.1379788.

527 [34] V.C. Nikolis, J. Benduhn, F. Holzmueller, F. Piersimoni, M. Lau, O. Zeika, D. Neher, C. Koerner,
528 D. Spoltore, K. Vandewal, Reducing Voltage Losses in Cascade Organic Solar Cells while
529 Maintaining High External Quantum Efficiencies, Adv. Energy Mater. 7 (2017) 1700855.
530 https://doi.org/10.1002/aenm.201700855.

531 [35] S. Ullbrich, J. Benduhn, X. Jia, V.C.V.C. Nikolis, K. Tvingstedt, F. Piersimoni, S. Roland, Y. Liu,
532 J. Wu, A. Fischer, D. Neher, S. Reineke, D. Spoltore, K. Vandewal, Emissive and charge-
533 generating donor–acceptor interfaces for organic optoelectronics with low voltage losses, Nat.
534 Mater. 18 (2019) 459–464. https://doi.org/10.1038/s41563-019-0324-5.

535 [36] H. Sasabe, D. Tanaka, D. Yokoyama, T. Chiba, Y.-J. Pu, K. Nakayama, M. Yokoyama, J. Kido,
536 Influence of Substituted Pyridine Rings on Physical Properties and Electron Mobilities of 2-
537 Methylpyrimidine Skeleton-Based Electron Transporters, Adv. Funct. Mater. 21 (2011) 336–342.
538 https://doi.org/10.1002/adfm.201001252.

539 [37] W. Zhao, A. Kahn, Charge transfer at n-doped organic-organic heterojunctions, J. Appl. Phys.
540 105 (2009) 123711. https://doi.org/10.1063/1.3153962.

541 [38] Fraunhofer FEP and Heliatek: Conclusion of BMBF research project on transparent organic
542 photovoltaic glass façades (TOP) - OPE Journal - Organic & Printed Electronics, (n.d.).
543 https://ope-journal.com/news/fraunhofer-fep-and-heliatek-conclusion-of-bmbf-research-
544 project-on-transparent-organic-photovoltaic-glass-facades-top (accessed May 21, 2021).

545 [39] Q. Burlingame, X. Huang, X. Liu, C. Jeong, C. Coburn, S.R. Forrest, Intrinsically stable organic

546   solar cells under high-intensity illumination, Nature. 573 (2019) 394–397.

547   https://doi.org/10.1038/s41586-019-1544-1.

548   [40]   S. Ben Dkhil, M. Pfannmöller, S. Bals, T. Koganezawa, N. Yoshimoto, D. Hannani, M. Gaceur,

549   C. Videlot-Ackermann, O. Margeat, J. Ackermann, Square-Centimeter-Sized High-Efficiency

550   Polymer Solar Cells: How the Processing Atmosphere and Film Quality Influence Performance

551   at Large Scale, Adv. Energy Mater. 6 (2016) 1600290. https://doi.org/10.1002/aenm.201600290.

552   [41]   S. Lenk, T. Schwab, S. Schubert, L. Müller-Meskamp, K. Leo, M.C. Gather, S. Reineke, White

553   organic light-emitting diodes with 4 nm metal electrode, Appl. Phys. Lett. 107 (2015) 163302.

554   https://doi.org/10.1063/1.4934274.

555   [42]   X. Xiao, K. Lee, S.R. Forrest, Inverted, semitransparent small molecule photovoltaic cells, Appl.

556   Phys. Lett. 107 (2015) 033901. https://doi.org/10.1063/1.4927142.

557   [43]   R.J. Peh, Y. Lu, F. Zhao, C.-L.K. Lee, W.L. Kwan, Vacuum-free processed transparent inverted

558   organic solar cells with spray-coated PEDOT:PSS anode, Sol. Energy Mater. Sol. Cells. 95 (2011)

559   3579–3584. https://doi.org/10.1016/j.solmat.2011.09.018.

560   [44]   C.J. Traverse, R. Pandey, M.C. Barr, R.R. Lunt, Emergence of highly transparent photovoltaics

561   for distributed applications, Nat. Energy. 2 (2017) 849–860. https://doi.org/10.1038/s41560-017-

562   0016-9.

563   [45]   L.T. Sharpe, A. Stockman, W. Jagla, H. Jägle, A luminous efficiency function, VD65* (λ), for

564   daylight adaptation: A correction, Color Res. Appl. 36 (2011) 42–46.

565   https://doi.org/10.1002/col.20602.

566   [46]   J. Hye Oh, S. Ji Yang, Y. Rag Do, Healthy, natural, efficient and tunable lighting: four-package

567   white LEDs for optimizing the circadian effect, color quality and vision performance, Light Sci.

568   Appl. 3 (2014) e141–e141. https://doi.org/10.1038/lsa.2014.22.

569   [47]   University of Minnesota, Windows for High-performance Commercial Buildings,

570   Commercialwindows.Org. (2011) 1–3. https://www.commercialwindows.org/shgc.php

571   (accessed September 9, 2020).

572   [48]   Window Selection Tool | Efficient Windows Collaborative, (n.d.).

573   https://www.efficientwindows.org/new-selection1/ (accessed November 13, 2020).

574   [49]   A. Piccolo, F. Simone, Performance requirements for electrochromic smart window, J. Build.

575   Eng. 3 (2015) 94–103. https://doi.org/10.1016/j.jobe.2015.07.002.

576   [50]   Window Technologies: Glazing Types - Double Low-E Glazing - Efficient Windows, (n.d.).

577   https://www.efficientwindows.org/gtypes-2lowe/ (accessed November 13, 2020).

578   [51]   C.-G. Granqvist, Out of a niche, Nat. Mater. 5 (2006) 89–90. https://doi.org/10.1038/nmat1577.

579   [52]   M.   Grätzel,   Ultrafast   colour   displays,   Nature.   409   (2001)   575–576.

580   https://doi.org/10.1038/35054655.

581   [53]   H.-H. Chou, A. Nguyen, A. Chortos, J.W. To, C. Lu, J. Mei, T. Kurosawa, W.-G. Bae, J.B.-H.

582   Tok, Z. Bao, A chameleon-inspired stretchable electronic skin with interactive colour changing

583   controlled by tactile sensing, Nat. Commun. 6 (2015) 8011. https://doi.org/10.1038/ncomms9011.

584   [54]   J.H.. Kwon, D.C. Choe, Smart window comprising electrochromic device and organic light-

585   emitting device, US 9,711,571 B2, 2017.

586   [55]   A.L. Dyer, R.H. Bulloch, Y. Zhou, B. Kippelen, J.R. Reynolds, F. Zhang, A Vertically Integrated

587   Solar-Powered Electrochromic Window for Energy Efficient Buildings, Adv. Mater. 26 (2014)

588   4895–4900. https://doi.org/10.1002/adma.201401400.

589   [56]   Y. Takahashi, A. Shirai, T. Segawa, T. Takahashi, K. Sakakibara, Why Does a Color-Developing

590   Phenomenon Occur on Thermal Paper Comprising of a Fluoran Dye and a Color Developer

591   Molecule?, Bull. Chem. Soc. Jpn. 75 (2002) 2225–2231. https://doi.org/10.1246/bcsj.75.2225.

592   [57]   G.W. Kim, R. Lampande, D.C. Choe, I.J. Ko, J.H. Park, R. Pode, J.H. Kwon, Next generation

593   smart window display using transparent organic display and light blocking screen, Opt. Express.

594   26 (2018) 8493. https://doi.org/10.1364/OE.26.008493.

595   [58]   R. Muthyala, Chemistry and Applications of Leuco Dyes, Springer US, Boston, MA, 2002.

596   https://doi.org/10.1007/b114004.

597   [59]   M. Yanagita, I. Aoki, S. Tokita, 13 C NMR and Electronic Absorption Spectroscopic Studies on

598   the Equilibrium between the Colorless Lactone and the Colored Zwitterion Forms of a Fluoran-

599   Based   Black   Color   Former,   Bull.   Chem.   Soc.   Jpn.   70   (1997)   2757–2763.

600   https://doi.org/10.1246/bcsj.70.2757.

601   [60]   M. Hojo, T. Ueda, M. Yamasaki, A. Inoue, S. Tokita, M. Yanagita, 1 H and 13 C NMR Detection

602   of the Carbocations or Zwitterions from Rhodamine B Base, a Fluoran-Based Black Color

603   Former, Trityl Benzoate, and Methoxy-Substituted Trityl Chlorides in the Presence of Alkali

604   Metal or Alkaline Earth Metal Perchlorates in Acet, Bull. Chem. Soc. Jpn. 75 (2002) 1569–1576.

605   https://doi.org/10.1246/bcsj.75.1569.

[61]   G. Cai, X. Cheng, M. Layani, A.W.M. Tan, S. Li, A.L.-S. Eh, D. Gao, S. Magdassi, P.S. Lee, Direct inkjet-patterning of energy efficient flexible electrochromics, Nano Energy. 49 (2018) 147–154. https://doi.org/10.1016/j.nanoen.2018.04.017.

[62]   Y. Wang, S. Wang, X. Wang, W. Zhang, W. Zheng, Y.-M. Zhang, S.X.-A. Zhang, A multicolour bistable electronic shelf label based on intramolecular proton-coupled electron transfer, Nat. Mater. 18 (2019) 1335–1342. https://doi.org/10.1038/s41563-019-0471-8.

[63]   W. Weng, T. Higuchi, M. Suzuki, T. Fukuoka, T. Shimomura, M. Ono, L. Radhakrishnan, H. Wang, N. Suzuki, H. Oveisi, Y. Yamauchi, A High-Speed Passive-Matrix Electrochromic Display Using a Mesoporous TiO2 Electrode with Vertical Porosity, Angew. Chemie. 122 (2010) 4048–4051. https://doi.org/10.1002/ange.200907008.

618   TOC Graphic:

619

620
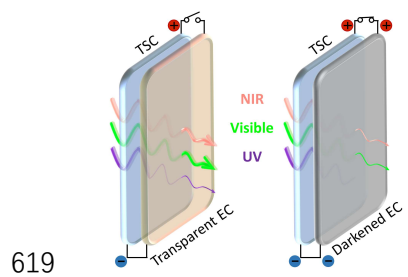
Highlights

- A prototype of a self-powered electrochromic smart window is demonstrated, which can dynamically modulate the sunlight transmission.

- Selectively UV-harvesting transparent solar cells (TSCs) show respectable average visible-light transmission (AVT, ~ 50-65%) and offer high photovoltages (1.5-2.0 V) to drive electrochromic devices.

- NIR-absorbing TSCs with an area of 2.52 cm^2 exhibit an efficiency of ~ 4% and an AVT of ~ 40%, which is the highest performance among reported small-molecule-based TSCs.

- High contrast ratio of electrochromic device over 80% in the range of 390 to 640 nm.